Infrared Frequency-Modulation Probing of Product Formation in Alkyl + O_2 Reactions: II. The Reaction of C_3H_7 with O_2 between 296 and 683 K

John D. DeSain,[†] Eileen P. Clifford,[†,‡] and Craig A. Taatjes*

Combustion Research Facility, Mail Stop 9055, Sandia National Laboratories, Livermore, California 94551-0969

Received: October 5, 2000; In Final Form: January 2, 2001

The production of HO_2 from the reaction of C_3H_7 and O_2 has been investigated as a function of temperature (296−683 K) using laser photolysis/CW infrared frequency-modulation spectroscopy. The HO_2 yield is derived by comparison with the $Cl_2/CH_3OH/O_2$ system and is corrected to account for HO_2 signal loss due to competing reactions involving HO_2 radical and the adduct $C_3H_7O_2$. The time behavior of the HO_2 signal following propyl radical formation was observed to have two separate components. The first component is a prompt production of HO_2, which increases with temperature and is the only HO_2 production observed between 296 and 550 K. This prompt yield increases from less than 1% at 296 K to ∼16% at 683 K. At temperatures above 550 K, a second, slower rise in the HO_2 signal is also observed. The production of HO_2 on a slower time scale is attributable to propylperoxy radical decomposition. The total HO_2 yield, including the contribution from the slower rise, increases rapidly with temperature from 5% at 500 K to 100% at 683 K. The second slower rise accounts for nearly all of the product formation at these higher temperatures. The biexponential time behavior of the HO_2 production from $C_3H_7 + O_2$ is similar to that previously observed in studies of the $C_2H_5 + O_2$ reaction. The temperature dependence of the prompt yield for the two reactions is very similar, with the $C_3H_7 + O_2$ reaction having a slightly lower yield at each temperature. The temperature dependence of the total HO_2 yield is also very similar for the two reactions, with the sharp increase in the total HO_2 yield at high temperatures occurring in very similar temperature ranges. The phenomenological rate constant for delayed HO_2 production from $C_3H_7 + O_2$ is slightly larger than that for $C_2H_5 + O_2$ at each temperature. Apparent activation energies, obtained from an Arrhenius plot of the inverse of the time constants for delayed HO_2 production, are similar for the two systems, being 24.6 and 26.0 kcal mol^{-1} for $C_2H_5 + O_2$ and $C_3H_7 + O_2$, respectively. These results suggest similar coupled mechanisms for HO_2 production in the $C_2H_5 + O_2$ and $C_3H_7 + O_2$ reactions, with similar concerted HO_2 elimination pathways from the RO_2 species.

Introduction

The reaction of alkyl radicals (R) with molecular oxygen is important in the oxidation of hydrocarbons in both combustion and atmospheric processes. The reaction of the propyl radical (C_3H_7) with O_2, like other R + O_2 reactions, has several product channels

$$C_3H_7 + O_2 \overset{M}{\leftrightarrow} C_3H_7O_2 \rightarrow \quad (1a)$$

$$\rightarrow C_3H_6 + HO_2 \quad (1b)$$

$$\rightarrow \textit{cyclo}\text{-}C_3H_6O \text{ (propylene oxide)} + OH \quad (1c)$$

where reactions 1b and 1c include possible formation from a $C_3H_7O_2$ intermediate. Recent experiments[1−6] have provided strong evidence that the $C_3H_7 + O_2$ reaction proceeds via a coupled mechanism, in which the formation of a propylperoxy adduct ($C_3H_7O_2$) is the initial step toward formation of all products. Slagle et al.[1] observed a negative temperature dependence for the removal rate coefficient of *i*-C_3H_7 with O_2 between 592 and 692 K and observed the *i*-$C_3H_7 + O_2 \leftrightarrow$ *i*-$C_3H_7O_2$ equilibrium. Slagle et al.[2] also measured a decrease in the rate coefficient with increasing temperature for the *n*-$C_3H_7 + O_2$ reaction between 297 and 635 K. Gulati and Walker[6] observed a negative activation energy between 653 and 773 K for the reaction of *i*-$C_3H_7 + O_2$. In that temperature range, the formation of C_3H_6 dominates the *i*-$C_3H_7 + O_2$ reaction, with only a small branching to OH + *c*-C_3H_6O (≤1%).[7] The observed negative temperature dependence for *i*-$C_3H_7 + O_2$ precludes an activated direct abstraction for reaction 1b. Kaiser and Wallington[4] found negative pressure dependence for the propylene yield from $C_3H_7 + O_2$ (yield ∝ $P^{-0.68\pm0.03}$), similar to the $P^{-0.8}$ dependence of the ethylene yield from $C_2H_5 + O_2$.[8−10] A pressure dependence of the product yield is expected if the products are formed by rearrangement of an excited propylperoxy adduct that can also be collisionally stabilized.

Of the R + O_2 reaction mechanisms, the reaction mechanism for ethyl radical (C_2H_5) has been the focus of the greatest number of recent experiments and theoretical calculations.[8−20] The $C_2H_5 + O_2$ reaction mechanism is often used as a convenient general model in oxidative mechanisms that include larger alkyl radicals, such as $C_3H_7 + O_2$. The evidence from these previous experiments and modeling studies indicates that $C_2H_5 + O_2$ proceeds via a coupled mechanism similar to the one proposed above for $C_3H_7 + O_2$. The formation of an excited ethylperoxy radical ($C_2H_5O_2$) is the initial reaction step. The

* Author to whom correspondence should be addressed.
[†] Sandia National Laboratories postdoctoral associate
[‡] Present address: Therma-Wave Inc., 1250 Reliance Way, Fremont, CA 94539

10.1021/jp0036543 CCC: $20.00
Published on Web 02/22/2001

ethylperoxy radical can either decompose to products or be collisionally stabilized.

$$C_2H_5 + O_2 \overset{M}{\leftrightarrow} C_2H_5O_2 \rightarrow \quad (2a)$$

$$\rightarrow C_2H_4 + HO_2 \quad (2b)$$

$$\rightarrow C_2H_4O \text{ (oxirane)} + OH \quad (2c)$$

In the first paper in this series,[11] the production of HO_2 for the reaction of ethyl + O_2 was investigated using laser photolysis/continuous-wave (CW) infrared (IR) frequency-modulation (FM) spectroscopy. The yield of HO_2 in the reaction was measured by comparing signals with a reference system (Cl_2/CH_3OH/O_2) that completely converts Cl atoms to HO_2. The HO_2 yield exhibited a biexponential time behavior with both a very fast direct component and a much slower delayed component. The prompt "direct" yield increases with temperature. The total yield rises sharply from ~10% to 100% between 575 and 675 K. The delayed component was observed to make a large contribution to the total yield at these higher temperature, while making no significant contribution at temperatures below 575 K. This biexponential time behavior could be predicted by using the parametrized model of Wagner et al.,[15] after correction for recent equilibrium constant data.[14] The yield and time behavior derived from recent master equation calculations by Miller, Klippenstein, and Robertson,[17] based on quantum calculations of the transition state for the concerted HO_2 elimination from the ethylperoxy radical,[16] also showed excellent agreement with the experimental results.[11]

The present study investigates the yield and time behavior of HO_2 formation from the C_3H_7 + O_2 reaction at elevated temperatures. Previous studies have observed the C_3H_6 product in this reaction. Kaiser et al.[4,5] performed end-product analysis from photolysis of Cl_2/C_3H_8/O_2 mixtures, using gas chromatography with flame-ionization detection. Using this method, Kaiser et al. were able to measure total yields but not the time dependence of the C_3H_6 formation. Slagle et al.,[1,2] using laser photolysis/time-resolved photoionization mass spectrometry, observed C_3H_6 from *n*-C_3H_7 + O_2 at 550 and 635 K but were forced to estimate the final propene yield at the higher temperature because of its slow rate of formation in the experiment.[2] Slagle et al. also had difficulty observing C_3H_6 formation from the *i*-C_3H_7 + O_2 reaction because of C_3H_6 production in the original photolysis. An upper limit for the yield in the *i*-C_3H_7 + O_2 system was reported at only one temperature (<7% at 500 K).[1]

In the current study, the time behavior of HO_2 formation from the reaction of C_3H_7 + O_2 is directly observed. A mixture of *n*- and *i*-C_3H_7 is formed by Cl atom reaction with propane, and the HO_2 formation is probed using infrared frequency-modulation spectroscopy. Measurement of the time profile of the HO_2 formation permits separation of initially formed prompt HO_2 from the product formed following thermal dissociation of the propylperoxy adduct. In this way, the increase in HO_2 + C_3H_6 yield above 550 K is unambiguously assigned to $C_3H_7O_2$ dissociation. The time behavior for the "delayed" formation of HO_2 is similar to that observed for C_2H_5 + O_2, which suggests that the two reactions have similar reaction mechanisms for HO_2 + alkene formation.

Experiment

The reaction of C_3H_7 + O_2 is investigated using a modification of the laser photolysis/CW infrared long-path absorption (LP/CWIRLPA) method, similar to that employed in previous experiments.[11,21−25] Cl is generated by photolysis of Cl_2 at 355 nm, and C_3H_7 is generated by subsequent Cl abstraction from propane. The C_3H_7 radical then reacts with O_2 to produce the HO_2 radical.

$$Cl_2 \xrightarrow{h\nu\ (355\ nm)} 2Cl\bullet \quad (3a)$$

$$Cl\bullet + C_3H_8 \rightarrow \bullet C_3H_7 + HCl \quad (3b)$$

$$\bullet C_3H_7 + O_2 \rightarrow \text{products} \quad (1)$$

The O_2 concentration is kept at least 30 times greater than the Cl_2 concentration in order to minimize the effects of the competing chain reaction of Cl_2 with C_3H_7. Both isomers of C_3H_7 are formed (*n*-propyl radical, $CH_3CH_2CH_2$, and *i*-propyl radical, CH_3CHCH_3), and no isomeric isolation was attempted in this experiment. Tschuikow-Roux et al.[26] measured the branching ratio of *i*-C_3H_7 to *n*-C_3H_7 produced from H abstraction by Cl from propane between 281 and 365 K. The branching ratios measured by Tschuikow-Roux et al.[26] extrapolate well to higher-temperature results (450−575 K) from unpublished experiments in our laboratory.[27]

An attempt to monitor possible OH production from reaction 1c by absorption on the P(2.5)1^- line of the vibrational fundamental[28] at 3484.6 cm^{-1} using an F-center laser proved unsuccessful at 668 K. A similar result was previously obtained from the C_2H_5 + O_2 study.[11] Walker and Morley[7] report about 1% OH from *i*-C_3H_7 + O_2 and 15% from *n*-C_3H_7 + O_2 at 750 K. Given our lower temperature and isomeric mixture of *i*-C_3H_7 and *n*-C_3H_7, the expected OH yield was near our observable limit. More detail on the OH detection limits of the apparatus are given in a previous publication.[11]

Apparatus. The progress of reaction 1b is monitored by infrared absorption of the overtone of the O−H stretch in HO_2 near 1.5 μm, first observed by Hunziker and Wendt,[29] using a tunable diode laser. Two-tone frequency modulation of the infrared lasers is sometimes employed to increase the signal-to-noise ratio. The detection sensitivity decreases at higher temperatures because of increases in the vibrational and rotational partition functions. The diode laser output is passed multiple times (17 passes) through a Herriott-type flow cell.[30,31] The flow cell is 1.3 m long, has CaF_2 windows, and is surrounded by a commercial ceramic-fiber heater capable of reaching temperatures in excess of 1200 K.

The gold-coated spherical mirrors of the Herriott cell are located outside the flow cell and are separated by a distance of approximately 1.5 m. A photolysis beam, a 5-ns pulse from a Nd:YAG laser at 355 nm, passes through a hole in the center of the front Herriott mirror. It travels on the axis through the quartz flow cell and passes again through a hole in the center of the back Herriott mirror. The IR probe beam enters off-axis through a notch in the back Herriott mirror and is passed multiple times through the flow cell. The beam traverses a circular pattern around the outer edge of the Herriott mirrors while mapping out a smaller circle in the center of the cell. Finally, the probe exits from a notch in the front Herriott mirror. After exiting, the probe beam is focused onto a detector. This arrangement allows the IR probe to intercept the UV photolysis beam only in the center of the flow cell, where the temperature is more readily controlled. Using this multipass arrangement, the effective path length (i.e., overlapping path of the photolysis and probe) is about 9 m.

The relative yield of the HO_2 radical produced by the reaction is monitored by comparison with the corresponding HO_2 yield from the reaction of CH_2OH + O_2. This reaction produces a

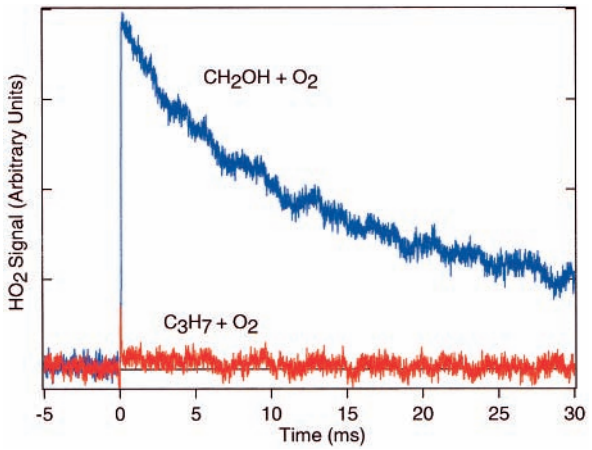

Figure 1. Time-resolved infrared FM signals for HO_2 taken at 473 K and 41.1 Torr. The blue, larger-amplitude trace is the HO_2 signal from the reference reaction of $CH_2OH + O_2$; the red, smaller-amplitude trace is the HO_2 signal from $C_3H_7 + O_2$. The yield at this temperature is estimated from the relative sizes of the sharp rise in the signal near $t = 0$.

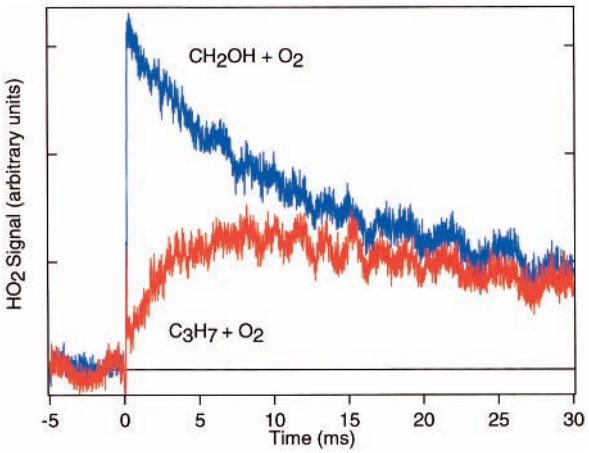

Figure 2. Time-resolved infrared FM signals for HO_2 taken at 645 K and 56.5 Torr. The blue, larger-amplitude trace is the HO_2 signal from the reference reaction of $CH_2OH + O_2$; the red, smaller-amplitude trace is the HO_2 signal from $C_3H_7 + O_2$.

100% yield of HO_2 as a product over the temperature range of concern.[32] The CH_2OH is produced by Cl abstraction of hydrogen from methanol.

$$Cl_2 \xrightarrow{h\nu\ (355\ nm)} 2Cl\bullet \qquad (4a)$$

$$CH_3OH + Cl\bullet \rightarrow CH_2OH\bullet + HCl \qquad 100\% \qquad (4b)$$

$$CH_2OH\bullet + O_2 \rightarrow CH_2O + HO_2\bullet \qquad 100\% \qquad (4c)$$

The experiments are conducted by first observing the HO_2 signal produced from the $CH_2OH + O_2$ reaction. Then the methanol is replaced with a nearly equal concentration of propane and the HO_2 signal from the $C_3H_7 + O_2$ reaction is observed. The yield is then obtained by comparison of the intensities of the two resulting HO_2 signals. To relate the observed quantities to characteristics of the reaction, corrections must be made for the removal reactions of HO_2, as well as for side reactions, as discussed below. Typical gas concentrations are 6.4×10^{16} cm^{-3} of O_2, 2.0×10^{15} cm^{-3} of Cl_2, and 8.0×10^{15} cm^{-3} of either propane or methanol. Helium is added to a total density of 8.45×10^{17} cm^{-3}.

Data Analysis. Figure 1 shows the HO_2 signals generated by the $CH_2OH + O_2$ and $C_3H_7 + O_2$ reactions at 473 K. From 296 to 550 K, the appearance of HO_2 occurs nearly instantaneously after the UV flash, as the O_2 and propane concentrations are high enough that production of C_3H_7 and reaction with O_2 occur very rapidly. However, at higher temperatures (>550 K), the HO_2 signal is seen to have an additional slower delayed rise. This delayed rise in the HO_2 signal at 645 K is clearly seen in Figure 2. At these higher temperatures (550−683 K), this second rise in the HO_2 signal prevents determination of the total HO_2 yield by simple comparison of the HO_2 signals from $CH_2OH + O_2$ and $C_3H_7 + O_2$. HO_2 radical recombination and reactions of the stabilized adduct reduce the HO_2 concentration on the time scale of the delayed signal rise. In addition, the effects of the $C_3H_7O_2$ recombination reactions (n-$C_3H_7O_2$ recombination, i-$C_3H_7O_2$ recombination, and i-$C_3H_7O_2$ + n-$C_3H_7O_2$ reaction) must be considered in order to model the $C_3H_7O_2$ concentration.

To correct the signal for the loss of HO_2, the integrated profiles technique is employed.[33−35] Correction for the self-reaction uses only information inherent to the HO_2 signals from $CH_2OH + O_2$ and $C_3H_7 + O_2$ and requires no assumed rate coefficients. The HO_2 signal generated from the $CH_2OH + O_2$ reaction decays by a second-order kinetic process dominated by the $HO_2 + HO_2$ recombination reaction.

$$HO_2 + HO_2 \rightarrow \text{products} \qquad (5)$$

The second-order rate can then be directly obtained from the $CH_2OH + O_2$ signal. The time profile of the HO_2 signal from the reference reaction is therefore given by

$$I_{ref}(t) = \alpha[HO_2]_t = \frac{\alpha[HO_2]_0}{1 + 2k_5 t[HO_2]_0} \qquad (6)$$

with α a that constant relates the HO_2 concentration to the FM signal amplitude. A plot of the inverse of the reference HO_2 signal vs time gives a line with slope $2k_5/\alpha$. Because the temperature-dependent line strength of the probe transition is unknown, the absolute value of k_5 remains undetermined in these experiments; however, the analysis requires only the phenomenological rate coefficient $2k_5/\alpha$. The differential equation governing the HO_2 concentration in the propyl + O_2 reaction can be written as

$$\frac{d}{dt}[HO_2] = R_{production} - 2k_5[HO_2]^2 - R_{removal} \qquad (7)$$

where $R_{production}$ and $R_{removal}$ are the effective time-dependent rate of HO_2 production and the effective time-dependent rate of removal of HO_2 by processes besides self-reaction, respectively. Determination of the time-resolved production of HO_2 from reaction 1, denoted $R_{production}$, is the aim of the measurement. Equation 7 has the formal solution

$$[HO_2]_t = \int_0^t R_{production}(x)\,dx - 2k_5\int_0^t [HO_2]_x^2\,dx - \int_0^t R_{removal}(x)\,dx \qquad (8)$$

The time-dependent FM signal from the HO_2 produced in reaction 1 can be described by

$$I(t) = \alpha\int_0^t R_{production}(x)\,dx - 2\alpha k_5\int_0^t [HO_2]_x^2\,dx - \alpha\int_0^t R_{removal}(x)\,dx \qquad (9)$$

TABLE 1: Reaction Rate Coefficients for $RO_2 + HO_2$ Reactions[a]

RO_2	reaction rate (cm^3 $molecule^{-1}$ s^{-1})
CH_3O_2[36]	4.83×10^{-12}
$C_2H_5O_2$[37]	7.28×10^{-12}
$CH_2{=}CHCH_2O_2$[38]	5.6×10^{-12}
$(CH_3)_3CCH_2O_2$[39]	1.47×10^{-11}
$C_5H_9O_2$[40]	1.52×10^{-11}
$C_6H_{11}O_2$[39]	1.70×10^{-11}
$C_6H_5CH_2O_2$[41]	1.01×10^{-11}

[a] All at 298 K except $CH_2{=}CHCH_2O_2$ at 393 K.

The integrated profiles method uses this formal solution, along with the measured time-resolved relative concentrations, to correct for known rate processes. In the present case, $2k_5/\alpha$ is known from the reference reaction, and the time profile of the HO_2 FM signal from reaction 1 has been measured as $I(t) = \alpha[HO_2]_t$. The self-reaction term in the expression for the FM signal amplitude, the second term on the right in eq 9, is thus simply related to the time integral of the observed signal by

$$2\alpha k_5 \int_0^t [HO_2]_x^2 \, dx = \frac{2k_5}{\alpha} \int_0^t I(x)^2 \, dx \qquad (10)$$

The "corrected" time profile is then given by eq 11.

$$\alpha \int_0^t R_{\text{production}}(x) \, dx = \frac{2k_5}{\alpha} \int_0^t I(x)^2 \, dx + \alpha \int_0^t R_{\text{removal}}(x) \, dx \qquad (11)$$

If HO_2 recombination were the only loss mechanism of significance, then R_{removal} would be equal to zero, and all of the parameters in eq 11 would be measured directly by the experiment. This assumption produces a lower limit to the actual HO_2 production rate, as additional corrections for HO_2 signal loss by other mechanisms (R_{removal}) will increase the amplitude of the final "corrected" time profile. The yields obtained by this assumption thus produce a lower limit to the true yields.

Whereas the data necessary for removing the contributions of the HO_2 self-reaction are inherent in the measurements themselves, additional modeling is required in relating the phenomenological yields to the time-dependent HO_2 production rate to account for the R_{removal} processes. Under the conditions of the present experiments, R_{removal} reflects principally reactions of HO_2 with $C_3H_7O_2$ radicals

$$HO_2 + C_3H_7O_2 \rightarrow \text{products} \qquad (12)$$

so that $R_{\text{removal}} \approx k_{12}[C_3H_7O_2]_t[HO_2]_t$. Unfortunately the $C_3H_7O_2 + HO_2$ reaction rate coefficients have not been measured previously. Table 1 lists available kinetic data for several $RO_2 + HO_2$ reactions; the rate coefficients for RO_2 species with 1−3 carbon atoms is about one-half to one-third that for species with 5−6 carbons. A value equal to that previously measured for the $C_2H_5O_2 + HO_2$ reaction was chosen to represent the rate constant for $C_3H_7 + O_2$. We also assume that both isomers of the propylperoxy radical will react in the same way with HO_2, as is the case for reactions involving propylperoxy with NO. The i-$C_3H_7O_2 + NO$ rate coefficient is reported as 2.7×10^{-12} $e^{(360/T)}$ cm^3 $molecule^{-1}$ s^{-1} and that for n-$C_3H_7O_2 + NO$ as 2.9×10^{-12} $e^{(350/T)}$ cm^3 $molecule^{-1}$ s^{-1}.[42,43]

Because the actual correction method uses the observed signals, not absolute concentrations, the value for the relevant rate coefficients must be scaled by the (unknown) factor α. The values for the rate coefficients (listed in Table 2) are therefore scaled to the literature value of the HO_2 recombination rate coefficient (whose phenomenological value, $2k_5/\alpha$, is measured in the $CH_2OH + O_2$ reference reaction), e.g.

$$\left(\frac{k_{12}}{\alpha}\right) = \left(\frac{2k_5}{\alpha}\right)\left(\frac{k_{12}}{k_5}\right)\frac{1}{2} \qquad (13)$$

Information on the concentration of $C_3H_7O_2$ is needed as well. Unfortunately, there is no direct measure of the time behavior of the propylperoxy radical concentration. An initial value is produced by assuming that all propyl radicals react with O_2 to produce either HO_2 or $C_3H_7O_2$. This assumption is valid if the steady state for reaction 1a favors the products, which is the case under the high-$[O_2]$ conditions of the present experiments. Then, immediately after the fast establishment of the steady-state concentration, $[C_3H_7O_2] \approx [C_3H_7]_0 - [HO_2]$. The concentration of $C_3H_7O_2$ is then modeled by integration of the rate equations forward in time, including the self-reaction of the propylperoxy radicals.

$$i\text{-}C_3H_7O_2 + i\text{-}C_3H_7O_2 \rightarrow \text{products} \qquad (14)$$

$$n\text{-}C_3H_7O_2 + n\text{-}C_3H_7O_2 \rightarrow \text{products} \qquad (15)$$

$$i\text{-}C_3H_7O_2 + n\text{-}C_3H_7O_2 \rightarrow \text{products} \qquad (16)$$

The two different isomers have differing recombination rate coefficients [$k_{14}(298\ K) = 3.3 \times 10^{-13}$ cm^3 $molecule^{-1}$ s^{-1} and $k_{15} = 1.70 \times 10^{-12}$ $e^{(-2190/T)}$ cm^3 $molecule^{-1}$ s^{-1}].[44,45] Thus, the composition of the propyl isomer mixture produced by Cl abstraction should be taken into account, making the procedure slightly different from that employed in the $C_2H_5 + O_2$ reaction.[11] The ratio of i-C_3H_7 to n-C_3H_7 produced is approximately 1:1 at room temperature and decreases slightly with increasing temperature.[26,27] The temperature dependence of the branching ratio is weak and should not change much over the temperature range of interest in this study (550−683 K).

The temperature dependence of n-$C_3H_7O_2$ recombination has not been studied previously. In the present analysis, a temperature dependence identical to that of the $C_2H_5O_2$ recombination is assumed. The rate coefficient for the n-$C_3H_7O_2 + i$-$C_3H_7O_2$ reaction is also unknown. The value used is an average of those for the n-$C_3H_7O_2$ recombination reaction and the i-$C_3H_7O_2$ recombination reaction. Using the n-$C_3H_7O_2$ recombination rate or the i-$C_3H_7O_2$ recombination rate alone in the analysis changes the yield by less than ±2% at 598 K. The rate of adduct recombination is then

$$R_{\text{recombination}} = 2k_{14}(0.45[C_3H_7O_2]_t)^2 + 2k_{15}(0.55[C_3H_7O_2]_t)^2 + k_{16}(0.55[C_3H_7O_2]_t)(0.45[C_3H_7O_2]_t) \qquad (17)$$

Using reactions 1, 5, 12, and 14−16, a formal solution to the kinetic equations can be constructed that allows recursive extraction of the time-resolved HO_2 production

$$\frac{d[C_3H_7O_2]}{dt} = -R_{\text{production}}(t) - R_{\text{recombination}}(t) - k_{12}[HO_2][C_3H_7O_2] \qquad (18)$$

$$[C_3H_7O_2]_t = [C_3H_7]_0 - \int_0^t R_{\text{production}}(x) \, dx - \int_0^t R_{\text{recombination}}(x) \, dx - k_{12}\int_0^t [C_3H_7O_2][HO_2] \, dx \qquad (19)$$

TABLE 2: Rate Coefficients Used to Obtain the Relative Rates Used to Correct the Yield Lost Due to the $C_3H_7O_2 + HO_2$ Reaction

reaction	rate coefficient (cm^3 molecule^{-1} s^{-1})
$HO_2 + HO_2$[12,a]	$k_5 = 4.5 \times 10^{-32}$ [M] $+ 2.2 \times 10^{-13}$ $e^{(599/T)}$
$C_3H_7O_2 + HO_2$[a]	$k_{12} = 6.9 \times 10^{-13}$ $e^{(702/T)}$
i-$C_3H_7O_2 + i$-$C_3H_7O_2$[45]	$k_{14} = 1.70 \times 10^{-12}$ $e^{(-2190/T)}$
n-$C_3H_7O_2 + n$-$C_3H_7O_2$[44,b]	$k_{15} = 5 \times 10^{-13}$ $e^{(-150/T)}$
n-$C_3H_7O_2 + i$-$C_3H_7O_2$[c]	$k_{16} = [1.70 \times 10^{-12}$ $e^{(-2190/T)} + 5 \times 10^{-13}$ $e^{(-150/T)}]/2$

[a] The evaluated rate coefficient for the HO_2 self-reaction is used to scale the value of the rate coefficient for $C_3H_7O_2 + HO_2$. The literature value for the $C_2H_5O_2 + HO_2$ rate coefficient is used as an estimate of the rate coefficient for $C_3H_7O_2 + HO_2$.[37] [b] The temperature dependence is an estimate based on the $C_2H_5O_2 + C_2H_5O_2$ reaction.[36] [c] Estimated as the mean of the i-$C_3H_7O_2$ and n-$C_3H_7O_2$ self-reaction rate coefficients.

The equation for the observed HO_2 FM signal is modified to reflect the fact that $R_{removal}$ is dominated by reaction with propylperoxy radicals, and as in previous work, the kinetic equations are recast as equations using the observed signals (i.e., effectively using signal amplitude as a concentration unit).

$$\alpha[C_3H_7O_2]_t = I_{ref}(0) - \alpha\int_0^t R_{production}(x)\,dx - \alpha\int_0^t R_{recombination}(x)\,dx - \frac{k_{12}}{\alpha}\int_0^t \alpha[C_3H_7O_2]I(x)\,dx \equiv A(t) \quad (20)$$

$$\alpha\int_0^t R_{production}(x)\,dx = I(t) + \frac{2k_5}{\alpha}\int_0^t I(x)^2\,dx + \frac{k_{12}}{\alpha}\int_0^t \alpha[C_3H_7O_2]_x I(x)\,dx \equiv B(t) \quad (21)$$

We initially assume $A_{(0)}(t) = 0$, and then calculate the nth approximations to the quantities $A(t)$ and $B(t)$ using the following equations:

$$B_{(n)}(t) = I(t) + \frac{2k_5}{\alpha}\int_0^t I(x)^2\,dx + \frac{k_{12}}{\alpha}\int_0^t A_{(n-1)}(x)I(x)\,dx \quad (22)$$

$$R_{recombination}(t) = \frac{2k_{14}}{\alpha}\{0.45[I_{ref}(0) - B_{(n)}(t)]^2\} + \frac{2k_{15}}{\alpha}\{0.55[I_{ref}(0) - B_{(n)}(t)]^2\} + \frac{k_{16}}{\alpha}\{0.55[I_{ref}(0) - B_{(n)}(t)]\}\{0.45[I_{ref}(0) - B_{(n)}(t)]\} \quad (23)$$

$$A_{(n+1)}(t) = [I_{ref}(0) - B_{(n)}(t)] - \int_0^t R_{recombination}(x)\,dx - \frac{k_{12}}{\alpha}\int_0^t [I_{ref}(0) - B_{(n)}(t)]I(x)\,dx \quad (24)$$

Iteration of these equations converges to a solution for $B(t)$, corresponding to the production of HO_2 from reaction 1 that would give rise to the observed signal under the conditions of the model. The yields extracted from this procedure are necessarily larger than the raw yields taken directly from the data (corrected only for HO_2 self-reaction). The yield estimates based on both methods (corrected only for HO_2 self-reaction and using $R_{removal} = k_{12}[C_3H_7O_2][HO_2]$) are given in Table 3 as Φ_{raw} and Φ_{total}, respectively.

Results

Figure 3 shows the HO_2 signals from both the $CH_2OH + O_2$ and $C_3H_7 + O_2$ reactions at 645 K after correction for the loss of signal due to HO_2 removal reactions. The HO_2 signal from the $CH_2OH + O_2$ reaction now appears to have a nearly instantaneous increase in HO_2 after the UV pulse, with no observable decrease in the signal over the 40-ms time window. The HO_2 signal from the $C_3H_7 + O_2$ reaction also differs from the raw signal in Figure 2. At the end of the second rise, the amplitude approaches a plateau. The total yield can now be obtained by a comparison of the final amplitude of the two signals. In practice, the HO_2 signal amplitude from $C_3H_7 + O_2$ is obtained by a simple fit of the HO_2 delayed rise to an exponential. More discussion of the biexponential behavior of the HO_2 signal appears below.

TABLE 3: Yields[a] and Time Constants[a] for HO_2 Production from $C_3H_7 + O_2$ at a Constant Density of 8.45×10^{17} cm^{-3}

temperature (K)	$1/\tau$ (s^{-1})	Φ_{prompt}	Φ_{raw}	Φ_{total}
296	–	<0.01	<0.01	<0.01
373	–	<0.01	<0.01	<0.01
473	–	0.04	0.04	0.04
500	–	0.04	0.04	0.04
550	39	0.03	0.09	0.20
573	56	0.08	0.09	0.30
598	66	0.05	0.18	0.43
610	88	0.08	0.22	0.51
623	140	0.06	0.30	0.55
638	170	0.12	0.44	0.69
645	213	0.09	0.51	0.75
653	255	0.10	0.60	0.86
660	331	0.18	0.69	0.88
668	450	0.11	0.91	0.94
683	602	0.16	1.00	1.00

[a] Values are the weighted means of four measurements at each listed temperature. Estimated relative uncertainties are ±10% for the total HO_2 yields, ±20% for the time constants, and ±40% for the prompt yields.

For comparison, Figure 3 also shows the HO_2 signal for the $C_3H_7 + O_2$ reaction obtained after correction for the HO_2 self-reaction only (green curve). This correction does not rely on any literature rate coefficients and is a lower bound to the actual HO_2 production. This signal is the basis of the "raw" HO_2 yield Φ_{raw}. If the rate of the cross-reaction $HO_2 + C_3H_7O_2$ were negligible, then this lower limit would be the correct yield. The correction for the removal of HO_2 by reaction with $C_3H_7O_2$, carried out by integration of the kinetic equations as described above, also yields a predicted $C_3H_7O_2$ time profile, which is shown by the violet trace.

The HO_2 product yield at a constant total density (8.45×10^{17} cm^{-3}) and constant partial densities of O_2, Cl_2, and methanol/propane for several different temperatures is shown in Figure 4. Each point in Figure 4 represents an average of four separate measurements. Table 3 lists the total yield of the raw data (Φ_{raw}), considering HO_2 self-reaction only, and the total yield considering all of the side reactions (Φ_{total}) at several different temperatures. The total yield of HO_2 is relatively small at temperatures below ~550 K. Above 550 K, a sharp increase in the total yield is observed in conjunction with a change in the time profile of the HO_2 signal. At these higher temperatures, the HO_2 signal has two rises, an instantaneous rise after the laser pulse followed by a slower secondary rise. The total yield reaches ~100% by about 683 K.

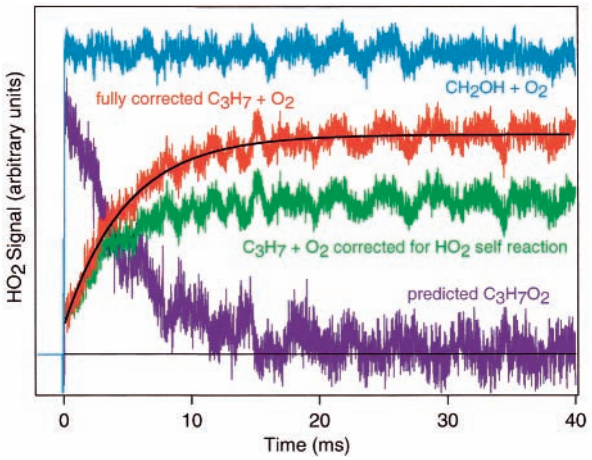

Figure 3. Correction of HO_2 FM signal using the integrated profiles method at 645 K and 56.5 Torr. The largest-amplitude trace (blue) is the HO_2 signal from the reference reaction of $CH_2OH + O_2$ after correction for HO_2 self-reaction, the dominant removal process for HO_2 in this system. The green $C_3H_7 + HO_2$ signal trace (smaller in amplitude) is the HO_2 signal after correction for only the HO_2 self-reaction, as described in the text. The red $C_3H_7 + HO_2$ signal trace (larger in amplitude) is the HO_2 signal after correction for both the HO_2 self-reaction and the reaction with $C_3H_7O_2$ radicals, as described in the text. The violet signal trace is the calculated adduct ($C_3H_7O_2$) signal, as predicted from the model used to correct the red $C_3H_7 + HO_2$ signal trace. The black line represents an exponential fit to the red $C_3H_7 + HO_2$ delayed HO_2 signal (the intercept corresponds to a prompt yield of 0.09 with a delayed production rate coefficient of $\tau^{-1} = 206\ s^{-1}$). These traces represents the time-resolved production of HO_2 corresponding to the observed time-resolved FM signals given in Figure 2.

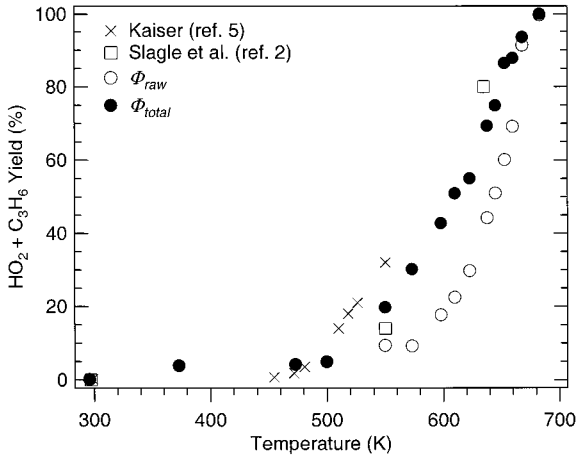

Figure 4. Measured total yield of HO_2 from the reaction of $C_3H_7 + O_2$ as a function of temperature at a constant total density of 8.45×10^{17} molecule cm^{-3}. The open circles (○) represent the total yield assuming only HO_2 self-reaction, which is a lower bound to the true HO_2 yield. The filled circles (●) represent the yield accounting for both the HO_2 self-reaction and the reaction with $C_3H_7O_2$ radicals, as described in the text. Also shown are the total yields obtained from previous experiments: the open squares (□) are from ref 2 and include only the *n*-C_3H_7 isomer; the crosses (×) are from ref 5 and include both isomers.

The assumptions made for various rate coefficients in the model used above puts a limit on the accuracy of the yields. The open circles in Figure 4 show the HO_2 yield if only the signal loss due to HO_2 recombination is replaced (which, again, entails no assumed rate coefficients). At higher temperatures, where replacing only the loss of signal due to HO_2 recombination already produces nearly unity yield, the more poorly known side reactions can have very little effect on the actual HO_2 signal.

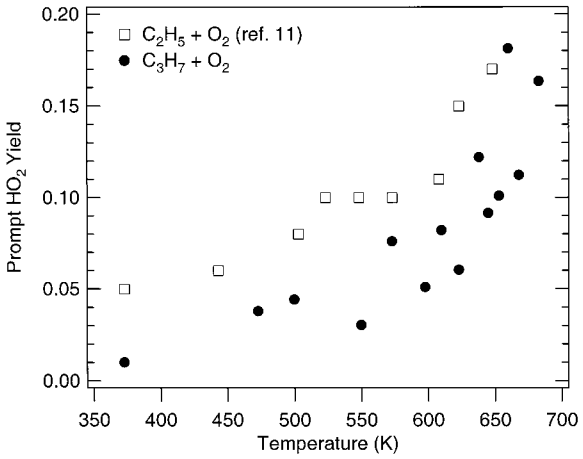

Figure 5. Temperature dependence of the prompt yield of HO_2 from the reactions of $C_3H_7 + O_2$ and $C_2H_5 + O_2$ at constant densities of 8.45×10^{17} and 7.7×10^{17} molecule cm^{-3}, respectively. The $C_3H_7 + O_2$ yields represented by filled circles (●) are from this work, while the open squares (□) represent the $C_2H_5 + O_2$ yields from ref 11.

At these temperatures, the dissociation of the $C_3H_7O_2$ radical, both back to reactants and forward to products, dominates over reactive removal of $C_3H_7O_2$. At lower temperatures, where no slow secondary rise of the HO_2 signal is observed, these side reactions also have very little effect on the yield. Thus, the high- and low-temperature limits of the HO_2 yield curve are well fixed, while the intermediate yields are subject to larger uncertainties. The $C_3H_7O_2 + HO_2$ reaction is the most important unknown rate coefficient. Table 1 lists the reaction rates of other RO_2 species with HO_2; the value of the rate coefficient chosen for $C_3H_7O_2 + HO_2$ is about one-half the largest rate coefficient in the table. It is unlikely that the rate coefficient for $C_3H_7O_2 + HO_2$ lies far outside the range of those for analogous $RO_2 + O_2$ reactions. The yield near the middle of the temperature range (610 K), where the results are most sensitive to the assumed rate coefficient for the $C_3H_7O_2 + HO_2$ reaction, can be recalculated using the largest $RO_2 + HO_2$ rate coefficient (that for $C_6H_{11}O_2 + HO_2$) in Table 1, which is more than double the value assumed in our analysis. This produces an increase in the total yield of ~9%. The ±10% error bars of the total HO_2 yield are therefore given as an estimate of the total accuracy, including errors introduced by the estimate of the $C_3H_7O_2 + HO_2$ rate coefficient.

Plotted in Figure 5 is the measured prompt yield of HO_2 determined from the amplitude of the initial rapid rise of the HO_2 signal. For small yields at lower temperatures where only this fast rise in HO_2 is observed, the initial noise tends to obscure the prompt yield, and the yield is estimated by an extrapolation of the signal decay back to $t = 0$. The prompt yield increases slightly with increasing temperature. At higher temperatures, it is occasionally hard to discern prompt yield from the initial slow HO_2 signal. At these temperatures, the intercept of an exponential fit to the slow HO_2 production is used to obtain the prompt yield. At temperatures above those of the present study, the prompt and delayed production become indistinguishable. The prompt yield (Φ_{prompt}) at several temperatures is listed in Table 3.

The time-resolved FM signal shown in Figure 3, after the correction for HO_2 self-reaction and $C_3H_7O_2 + HO_2$ reactions, is related to the production of HO_2 in reaction 1.

$$I_{eff}(t) \approx \alpha \int_0^t R_{production}(x)\, dx \qquad (25)$$

The present experiments require relatively large concentrations

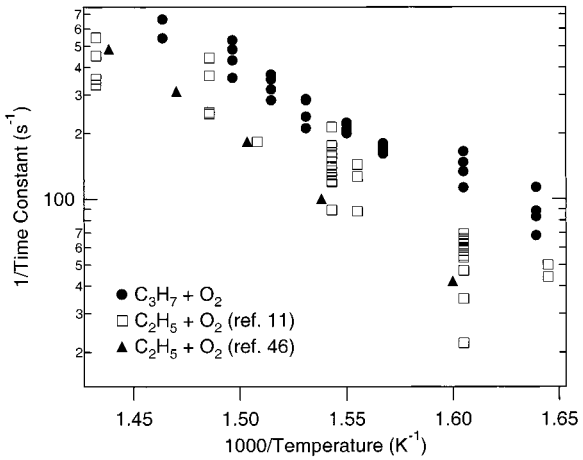

Figure 6. Arrhenius plot of the rate of formation (τ^{-1}) for delayed production of HO_2 from the reactions of $C_3H_7 + O_2$ and $C_2H_5 + O_2$ at constant densities of 8.45×10^{17} and 7.7×10^{17} molecule cm^{-3}, respectively. The $C_3H_7 + O_2$ rate of formation represented by filled circles (●) are from this work, while the open squares □ represent the $C_2H_5 + O_2$ rate of formation from ref 11. The triangles (▲) represent the rate of formation predicted by master equation calculations for $C_2H_5 + O_2$.[46]

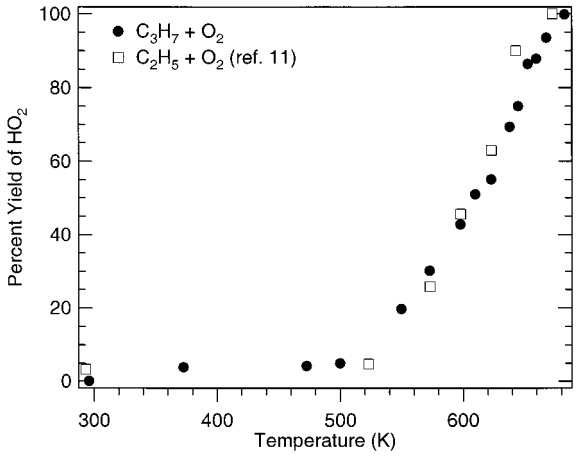

Figure 7. Comparison of the HO_2 yield of the propyl + O_2 and ethyl + O_2 reactions as a function of temperature. The filled circles (●) show the measured total yield of HO_2 from the reaction of $C_3H_7 + O_2$ as a function of temperature at a constant total density of 8.45×10^{17} molecule cm^{-3}. The open squares (□) show the measured total yield of HO_2 from the reaction of $C_2H_5 + O_2$ as a function of temperature at a constant total density of 7.7×10^{17} molecule cm^{-3} from ref 11.

of O_2, as the signal size is determined by the initial Cl concentration (and hence the Cl_2 concentration) and $[O_2]$ is maintained at $30[Cl_2]$. As a result, the initial rise of HO_2 from the reaction of propyl radical with O_2 is rapid and unresolved. However, the slower rate of formation in the production of HO_2 can be measured using an exponential fit, and the rates of formation are listed in Table 3 (note that this quantity, the inverse of a time constant, is inaccurately referred to as a time constant in ref 11). Figure 6 shows a semilogarithmic plot of τ^{-1} extracted from the signals, after correction for the self-reaction and the $HO_2 + C_3H_7O_2$ reaction (and reactions 14−16), as a function of inverse temperature. The rate of formation displays a rapid increase from approximately 39 s^{-1} at 550 K to several hundred per second at 683 K. The lowest temperature production rates are slightly affected by the correction for reaction 12, but at higher temperatures, this correction is less important, and the time constants are independent of the details of the HO_2 removal mechanism.

Discussion

Figure 4 compares the present yield measurements with several previous determinations. The product yield measurements (obtained by detecting the C_3H_6 from reaction 1c) by Slagle et al.[2] were made for *n*-$C_3H_7 + O_2$ only. For the *i*-$C_3H_7 + O_2$ reaction, Slagle et al.[1] concluded that there was not a significant homogeneous reaction leading to C_3H_6 formation in their experiments. At 635 K, the C_3H_6 yield from *n*-$C_3H_7 + O_2$ was estimated by Slagle et al.[2] to be >80%. The product yield of 69% at 638 K from the present study is somewhat lower than this value, although this intermediate-temperature determination depends on the assumed rate coefficient for reaction 13. If no HO_2 were generated by *i*-$C_3H_7 + O_2$ then 69% is somewhat larger than what would be expected, given that only ~55% of the C_3H_7 radicals generated in this experiment are *n*-C_3H_7. The *i*-$C_3H_7 + O_2$ reaction appears to be contributing to the total HO_2 yield at these higher temperatures. In fact, a ~100% total HO_2 yield from this experiment is impossible without significant contributions from both isomers. Slagle et al.[14] have recently reanalyzed their equilibrium results for *i*-$C_3H_7 + O_2$ by including homogeneous reaction losses of *i*-$C_3H_7O_2$; however, no new estimate has been made of alkene formation in that reaction.

Figure 4 shows a discrepancy between the temperature dependence of Kaiser's C_3H_6 yield[5] and the present HO_2 yield results. The temperature ranges in which the product yield begins its rapid increase differ by about 30−40 K. A similar discrepancy was previously observed for the $C_2H_5 + O_2$ reaction.[11] Because the reactive removal of alkylperoxy radicals, which competes with dissociation back to reactants or on to HO_2 + alkene products, is dominated by radical−radical reactions, the observed yield is sensitive to radical density. As in the case of $C_2H_5 + O_2$, the different radical densities used in Kaiser's studies and the time-resolved infrared FM measurements can explain the differences in product yield.

Figure 7 shows the total HO_2 product yield at different temperatures from the $C_3H_7 + O_2$ reaction and the $C_2H_5 + O_2$ reaction obtained by observing HO_2 formation. The studies were done at slightly different total densities (8.45×10^{17} and 7.7×10^{17} cm^{-3}, respectively). The total HO_2 product yields from both reactions have nearly identical temperature dependences. To describe the dynamics of reaction 2, Wagner et al.[15] used a simplified analytical model, in which the measured quantities (the dependence of the time behavior of the HO_2 yields on temperature and pressure) can be related to explicit convolution of elementary kinetic steps. Reaction 2 proceeds through the intermediate $C_2H_5O_2$, and a simplified formal kinetic scheme for the reaction can be constructed using only the species in reactions 2a−c

$$C_2H_5 + O_2 \xrightarrow{k_a} C_2H_4 + HO_2 \qquad (26)$$

$$C_2H_5 + O_2 \underset{k_{2a}[M]}{\longleftrightarrow} C_2H_5O_2 \xrightarrow{k_e[M]} C_2H_4 + HO_2 \qquad (27)$$

$$\downarrow$$

$$\textit{removal}$$

where k_e represents the rate constant for elimination from thermalized $C_2H_5O_2$ and k_a represents the rate constant for direct production of HO_2 and ethylene from the reactants. According to the current understanding of the $C_2H_5 + O_2$ potential energy surface, this direct production is best described as concerted

elimination of the HO_2 from the excited ethylperoxy adduct prior to stabilization.[16,17] In general, the kinetics of the reaction scheme (26, 27) gives a biexponential production of HO_2 products, where the rate of formation and amplitudes depend on all of the rate coefficients of the system. This phenomenological scheme reproduces the biexponential behavior of the HO_2 yields from $C_2H_5 + O_2$.

The HO_2 yields from the present experiment once again demonstrate this biexponential time behavior. Similarly to $C_2H_5 + O_2$, the first exponential can not be temporally resolved under these experimental conditions and results in the appearance of prompt HO_2 formation, but the second exponential can be resolved and is fit to an exponential to obtain the rate of formation τ^{-1}. One difference between the model (eq 26, 27) used for $C_2H_5 + O_2$ and one that could describe the $C_3H_7 + O_2$ reaction is that the $C_3H_7 + O_2$ model would need to consider the fate of the two isomers of $C_3H_7O_2$, *n*-$C_3H_7O_2$ and *i*-$C_3H_7O_2$. Instead of a single exponential observed for $C_2H_5 + O_2$, the delayed yield for $C_3H_7 + O_2$ would, in general, be the sum of two exponentials in such a model. However, a biexponential fit to the delayed yield from $C_3H_7 + O_2$ did not result in a better fit than a single exponential. Thus, the rates of formation of delayed HO_2 from the two propylperoxy isomers are too similar to be resolved in this experiment, and a single exponential is chosen for the rate of production.

As seen in Figure 5, the prompt yields from $C_2H_5 + O_2$ and $C_3H_7 + O_2$ show similar temperature dependences. The prompt HO_2 yield from $C_3H_7 + O_2$ is lower at all temperatures than the prompt yield from $C_2H_5 + O_2$, despite the significant scatter in the measurements. Kaiser and Wallington[4] previously observed that alkene production from $C_3H_7 + O_2$ is lower than that from $C_2H_5 + O_2$ at 298 K. They postulated that the smaller alkene yield for $C_3H_7 + O_2$ is due to more efficient stabilization of the propylperoxy radical than the ethylperoxy radical because of the additional vibrational degrees of freedom in the propylperoxy radical. Although the uncertainty in the present measurements of low-temperature prompt yields is considerably greater than that of Kaiser and Wallington's product yield measurements, the results are consistent with their interpretation.

As shown in Figure 6, the rate of delayed HO_2 formation is slightly larger at each temperature for $C_3H_7 + O_2$ than for $C_2H_5 + O_2$. Also shown in Figure 6 are rates of formation of the delayed yield predicted by calculations based on master equation calculations by Miller et al.[46] The master equation calculations employ two transition states. The first transition state (TS1) on the reaction path between $C_2H_5 + O_2$ and $C_2H_5O_2$, reflecting the establishment of the steady state between addition and redissociation, governs the fast time constant. The second transition state (TS2) is for direct elimination of HO_2 from $C_2H_5O_2$. In the master equations, the energy of TS2 is taken to be -4.3 kcal mol^{-1} from the energy of the reactants ($C_2H_5 + O_2$).[15,18,20] The second transition state completely determines the high-temperature rate coefficient as stabilization becomes negligible, and Miller et al. adjusted the energy of this transition state by $\sim$1.3 kcal mol^{-1} from their ab initio calculation of -3 kcal mol^{-1} in order to match high-temperature rate coefficient data. The rates of production predicted in their calculations show excellent agreement with measured time constants for $C_2H_5 + O_2$. The rate of formation of HO_2 for $C_3H_7 + O_2$ is slightly larger at each temperature, which could in principle reflect different falloff behavior for the two reactions. However, the previous experiments on $C_2H_5 + O_2$ show that this rate of formation is already pressure-independent.[11] Figure 8 shows measurements of the rate of formation for $C_3H_7 + O_2$,

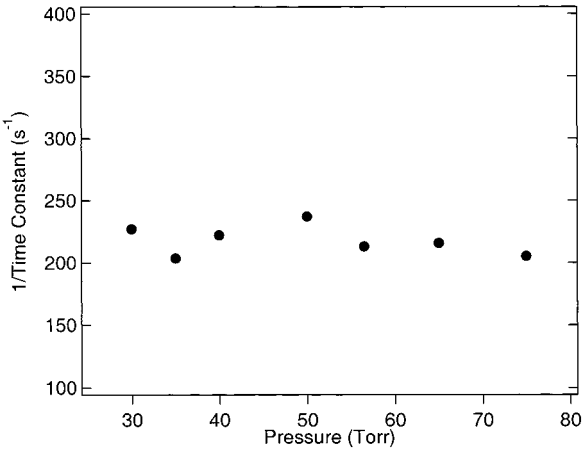

Figure 8. Pressure dependence of the rate of formation, τ^{-1}, for delayed production of HO_2 from the reaction of $C_3H_7 + O_2$ at a constant O_2 density of 6.4×10^{16} molecule cm^{-3} and at 645 K. Each point represents an average of four separate measurements.

establishing that it is also pressure-independent at 645 K between 30 and 75 Torr. The lack of pressure dependence of τ^{-1} under these conditions excludes the possibility that the rate of formation is greater for $C_3H_7 + O_2$ than for $C_2H_5 + O_2$ because it is nearer the high-pressure limit.

Although the rates of formation at each temperature are slightly larger for $C_3H_7 + O_2$, both reactions have similar apparent activation energies of the delayed yield. The similarity in the apparent activation energies of the two reactions can be seen from the Arrhenius plot (Figure 6). The apparent activation energies are 24.6 and 26.0 kcal mol^{-1} for $C_2H_5 + O_2$ and $C_3H_7 + O_2$, respectively. As seen from the reaction scheme (eq 26, 27), this delayed production rate cannot be isolated to a single rate constant in the reaction but rather is dependent, to some degree, on all of the rate coefficients. Thus, this measured activation energy is not an isolated measurement of a single energy barrier of any one step in the reaction but a phenomenological activation energy for the whole mechanism leading to delayed product formation. The similar temperature dependences of these reactions appear to imply similar energetics for HO_2 elimination, suggesting that analogous concerted elimination transition states are important. A fit to the rate of formation predicted by the master equation calculations yields a slightly larger apparent activation energy of 29.5 kcal mol^{-1} for $C_2H_5 + O_2$. The time constants have a strong dependence on the energy of TS2 for $C_2H_5 + O_2$. Further theoretical studies aimed at describing the potential energy surface of the $C_3H_7 + O_2$ reaction are needed to help illuminate details of its mechanism.

Conclusion

The reaction of propyl radicals with O_2 has been investigated as a function of temperature between 296 and 683 K using laser photolysis/CW frequency-modulation spectroscopy. The overall yield of HO_2 from the propyl radical + O_2 reaction has been observed as a function of temperature. The HO_2 occurs on two different time scales: a prompt HO_2 signal is observed immediately following the UV flash, and a second slower rise is also observed at higher temperatures. The total yield is compatible with the product yields previously determined by observation of the reaction product C_3H_6. The results from the $C_3H_7 + O_2$ reaction are similar to the previous results obtained from the $C_2H_5 + O_2$ reaction. The previous paper in this series demonstrated that product formation from $C_2H_5 + O_2$ shows excellent agreement with the predictions from a coupled kinetics

model, in which the formation of an ethylperoxy radical is the antecedent to ethylene + HO_2 formation. The present paper clearly shows the strong similarity of HO_2 product formation from the reactions of $C_2H_5 + O_2$ and $C_3H_7 + O_2$. This similarity suggests that $C_3H_7 + O_2$ must undergo a similar coupled kinetics scheme, in which propylperoxy radical is the antecedent to propylene + HO_2 formation. The apparent activation energies of the two reactions are also very similar, which suggests that the relative energies of the two reactions' transition states might be similar as well. Further theoretical studies aimed at describing the potential energy surface of the $C_3H_7 + O_2$ reaction could help to clarify the results.

Acknowledgment. The experiments described herein were made possible by the able technical support of Leonard E. Jusinski. We thank Dr. James A. Miller and Dr. Stephen J. Klippenstein for communicating results prior to publication. This work is supported by the Division of Chemical Sciences, Office of Basic Energy Science, U.S. Department of Energy.

References and Notes

(1) Slagle, I. R.; Ratajczak, E.; Heaven, M. C.; Gutman, D.; Wagner, A. F. *J. Am. Chem. Soc.* **1985**, *107*, 1838.
(2) Slagle, I. R.; Park, J.; Gutman, D. *Proc. Combust. Inst.* **1985**, *20*, 733.
(3) Ruiz, R. P.; Bayes, K. D. *J. Phys. Chem.* **1984**, *88*, 2592.
(4) Kaiser, E. W.; Wallington, T. J. *J. Phys. Chem.* **1996**, *100*, 18770.
(5) Kaiser, E. W. *J. Phys. Chem.* **1998**, *102*, 5903.
(6) Gulati, S. K.; Walker, R. W. *J. Chem. Soc., Faraday Trans. 2* **1988**, *84* (4), 401−407.
(7) Walker, R. W.; Morley, C. In *Low-Temperature Combustion and Autoignition*; Pilling, M. J., Ed.; Elsevier: Amsterdam, 1997; Vol. 35, p 1.
(8) Kaiser, E. W. *J. Phys. Chem.* **1995**, *99*, 707.
(9) Kaiser, E. W.; Lorkovic, I. M.; Wallington, T. J. *J. Phys. Chem.* **1990**, *94*, 3352.
(10) Kaiser, E. W.; Wallington, T. J.; Andino, J. M. *Chem. Phys. Lett.* **1990**, *168*, 309.
(11) Clifford, E. P.; Farrell, J. T.; DeSain, J. D.; Taatjes, C. A. *J. Phys. Chem. A* **2000**, *104*, 11549.
(12) Atkinson, R.; Baulch, D. L.; Cox, R. A.; Hampson, R. F., Jr.; Kerr, J. A.; Rossi, M. J.; Troe, J. *J. Phys. Chem. Ref. Data* **1997**, *26*, 521.
(13) Kaiser, E. W.; Rimai, L.; Wallington, T. J. *J. Phys. Chem.* **1989**, *93*, 4094.
(14) Knyazev, V. D.; Slagle, I. R. *J. Phys. Chem. A* **1998**, *102*, 1770.
(15) Wagner, A. F.; Slagle, I. R.; Sarzynski, D.; Gutman, D. *J. Phys. Chem.* **1990**, *94*, 1853.
(16) Rienstra-Kiracofe, J. C.; Allen, W. D.; Schaefer, H. F., III. *J. Phys. Chem. A* **2000**, *104*, 928. Ignatynev, I. S.; Xie, Y.; Allen, W. D.; Schaefer, H. F., III. *J. Chem. Phys.* **1997**, *107*, 141.
(17) Miller, J. A.; Klippenstein, S. J.; Robertson, S. H. *Proc. Combust. Inst.* **2000**, *28*, in press.
(18) Slagle, I. R.; Feng, Q.; Gutman, D. *J. Phys. Chem.* **1984**, *88*, 3648.
(19) McAdam, K. G.; Walker, R. A. *J. Chem. Soc., Faraday Trans. 2* **1987**, *83*, 1509.
(20) Slagle, I. R.; Ratajczak, E.; Gutman, D. *J. Am. Chem. Soc.* **1985**, *107*, 1838.
(21) Pilgrim, J. S.; Taatjes, C. A. *J. Phys. Chem. A* **1997**, *101*, 5776.
(22) Pilgrim, J. S.; Taatjes, C. A. *J. Phys. Chem. A* **1997**, *101*, 4172.
(23) Pilgrim, J. S.; McIlroy, A.; Taatjes, C. A. *J. Phys. Chem. A* **1997**, *101*, 1873.
(24) Pilgrim, J. S.; Taatjes, C. A. *J. Phys. Chem. A* **1997**, *101*, 8741.
(25) Farrell, J. T.; Taatjes, C. A. *J. Phys. Chem. A* **1998**, *102*, 4846.
(26) Tschuikow-Roux, E.; Yano, T.; Niedzielski, J. *J. Chem. Phys.* **1985**, *82* (1), 65.
(27) Taatjes, C. A. Unpublished data. Measurements of rate coefficients and HCl yields from reactions of Cl with partially deuterated propanes suggest an *n*-propyl branching fraction of 0.53 ± 0.16 at 575 K.
(28) Maillard, J. P.; Chauville, J.; Mantz, A. W. *J. Mol. Spectrosc.* **1976**, *63*, 120.
(29) Hunziker, H. E.; Wendt, H. R. *J. Chem. Phys.* **1974**, *60*, 4622.
(30) Herriott, D.; Kogelnik, H.; Kompfner, R. *Appl. Opt.* **1964**, *3*, 523.
(31) Pilgrim, J. S.; Jennings, R. T.; Taatjes, C. A. *Rev. Sci. Instrum.* **1997**, *68*, 1875.
(32) DeMore, W. B.; Sander, S. P.; Golden, D. M.; Hampson, R. F.; Kurylo, M. J.; Howard, C. J.; Ravishankara, A. R.; Kolb, C. E.; Molina, M. J. *Chemical Kinetics and Photochemical Data for Use in Stratospheric Modeling*; JPL Publication 97-4; Jet Propulsion Laboratory: Pasadena, CA, 1997.
(33) Yamasaki, K.; Wantanabe, A.; Kakuda, T.; Ichikawa, N.; Tokue, I. *J. Phys. Chem. A* **1999**, *103*, 451.
(34) Yamasaki, K.; Wantanabe, A. *Bull. Chem. Soc. Jpn.* **1997**, *70*, 89.
(35) Yamasaki, K.; Wantanabe, A.; Kakuda, T.; Tokue, I. *Int. J. Chem. Kinet.* **1998**, *30*,
(36) Wallington, T. J.; Dagaut, P.; Kurylo, M. J. *Chem. Rev.* **1992**, *92*, 667.
(37) Maricq, M.; Szente, J. J. *J. Phys. Chem.* **1994**, *98*, 2078.
(38) Boyd, A. A.; Noziere, B.; Lesclaux, R. *J. Chem. Soc., Faraday Trans.* **1996**, *92*, 201.
(39) Rowley, D. M.; Lesclaux, R.; Lightfoot, P. D.; Hughes, K.; Hurley, M. D.; Rudy, S.; Wallington, T. J. *J. Phys. Chem.* **1992**, *96*, 7043.
(40) Crawford, M. A.; Szente, J. J.; Maricq, M. M.; Francisco, J. S. *J. Phys. Chem. A* **1997**, *101*, 5337.
(41) Noziere, B.; Lesclaux, R.; Hurley, M. D.; Dearth, M. A.; Wallington, T. J. *J. Phys. Chem.* **1994**, *98*, 2864.
(42) Eberhard, J.; Howard, C. J. *Int. J. Chem. Kinet.* **1996**, *28*, 731.
(43) Eberhard, J.; Villalta, P. W.; Howard, C. J. *J. Phys. Chem.* **1996**, *100*, 993.
(44) Adachi, H.; Basco, N. *Int. J. Chem. Kinet.* **1982**, *14*, 1125.
(45) Kirsch, L. J.; Parkes, D. A.; Waddington, D. J.; Woolley, A. *J. Chem. Soc., Faraday Trans. 1* **1978**, *74*, 2293.
(46) Miller, J. A.; Klippenstein, S. J., submitted for publication.